Metal Phthalocyanine Nanoribbons and Nanowires

W. Y. Tong, A. B. Djurišić,* M. H. Xie, A. C. M. Ng, and K. Y. Cheung

Department of Physics, University of Hong Kong, Pokfulam Road, Hong Kong

W. K. Chan and Y. H. Leung

Department of Chemistry, University of Hong Kong, Pokfulam Road, Hong Kong

H. W. Lin and S. Gwo

Department of Physics, National Tsing Hua University, Hsinchu 300, Taiwan

Received: May 15, 2006; In Final Form: July 19, 2006

Nanoribbons and nanowires of different metal phthalocyanines (copper, nickel, iron, cobalt, and zinc), as well as copper hexadecafluorophthalocyanine (F_{16}CuPc), have been grown by organic vapor-phase deposition. Their properties, as a function of substrate type, source-to-substrate distance, and substrate temperature, were studied by scanning electron microscopy, transmission electron microscopy, X-ray diffraction, and absorption measurements. The size and morphology of the nanostructures were found to be mainly determined by the substrate temperature. The crystal structure was dependent on the substrate temperature as well. At substrate temperatures below 200 °C, in addition to straight nanoribbons, twisted nanoribbons were found for all investigated materials except F_{16}CuPc, which formed helical nanoribbons upon exposure to an electron beam. The formation of different nanostructures (nanoribbons, twisted nanoribbons, and helical nanoribbons) is discussed.

1. Introduction

Metal phthalocyanines are porphyrin derivatives consisting of a central metallic atom bound to a π-conjugated ligand, characterized by high symmetry, planarity, and electron delocalization.[1] They have attracted a great deal of attention for a wide variety of applications, such as solar cells,[1−3] organic light-emitting diodes as hole-transport or buffer layers[4−6] and infrared-emitting layers,[7] field-effect transistors (FETs),[8−12] and gas sensors.[13−15] Therefore, the optical properties,[16−23] structure, and growth[24−39] of metal phthalocyanines have been extensively studied. Among a number of different metal phthalocyanines, copper phthalocyanine (CuPc) has been most extensively studied.[1] The properties of other metal phthalocyanines have been studied less extensively than those of CuPc, but their structural and optical properties have been previously reported. On the other hand, studies of metal phthalocyanine derivatives such as copper hexadecafluorophthalocyanine (F_{16}CuPc) have been scarce.[38,39] Unlike unsubstituted metal phthalocyanines, which exhibit p-type conductivity, F_{16}CuPc exhibits n-type conductivity, which is of great interest for practical applications.[10,38]

Although it has been shown that some degree of orientation in metal phthalocyanine films can be induced on specific substrates and for specific deposition conditions,[24,32] the films prepared by thermal evaporation are typically polycrystalline with random orientation of the crystal grains. The consequence of this polycrystallinity is a high density of defects and a low carrier mobility due to the existence of disorder and grain boundaries.[12] One possible solution for this problem is the use of single-crystalline metal phthalocyanine micro- or nanostructures instead of polycrystalline thin films. Promising results have been reported recently for organic field-effect transistors based on single-crystalline CuPc ribbons,[12] as well as for organic solar cells with a nanostructured CuPc layer.[3] CuPc nanostructures can be fabricated using templates such as porous alumina[40] or by organic vapor-phase deposition (OVPD).[3,12] The OVPD method can be used to fabricate organic millimeter-sized crystals,[41] thin films,[42] or nanostructures.[3,12,43,44] Horizontal[3,12,44] and vertical[43] geometries can both be used for fabricating organic nanostructures. To date, CuPc nanorods (α phase)[3] and submicrometer-sized ribbons (β phase)[12] have been reported. However, there has been no systematic study of the growth of phthalocyanine nanostructures using the OVPD method.

Herein, we investigate the growth process and properties of nanoribbons and nanowires of five metal phthalocyanines: CuPc, cobalt phthalocyanine (CoPc), nickel phthalocyanine (NiPc), iron phthalocyanine (FePc), and zinc phthalocyanine (ZnPc). We found that the crystal phase and nanostructure size are strongly dependent on the substrate temperature. All investigated metal phthalocyanines exhibit similar morphologies in general, but there are small differences in the precise temperatures at which a certain morphology occurs for different metal phthalocyanines. In addition to very long β-phase nanoribbons found at high substrate temperatures and α-phase nanowires found at low substrate temperatures, twisted α-phase nanoribbons were obtained. In addition to the growth of different metal phthalocyanine nanostructures, growth of an n-type phthalocyanine derivative, F_{16}CuPc, was studied. In this case, the obtained morphologies were also strongly dependent on the substrate temperature, but no twisted nanoribbons were found. However, helical nanoribbons of F_{16}CuPc were formed upon exposure to an electron beam inside a scanning electron microscope (SEM).

* To whom correspondence should be addressed. E-mail: dalek@hkusua.hku.hk.

10.1021/jp062951q CCC: $33.50
Published on Web 08/17/2006

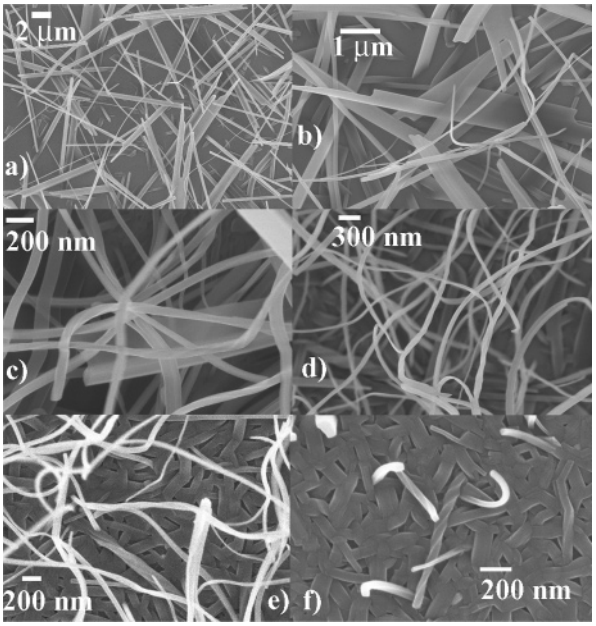

Figure 1. Representative SEM images of CuPc nanostructures on glass substrates for different substrate temperatures (a) 240, (b) 216, (c) 195, (d) 170, (e) 142, and (f) 119 °C.

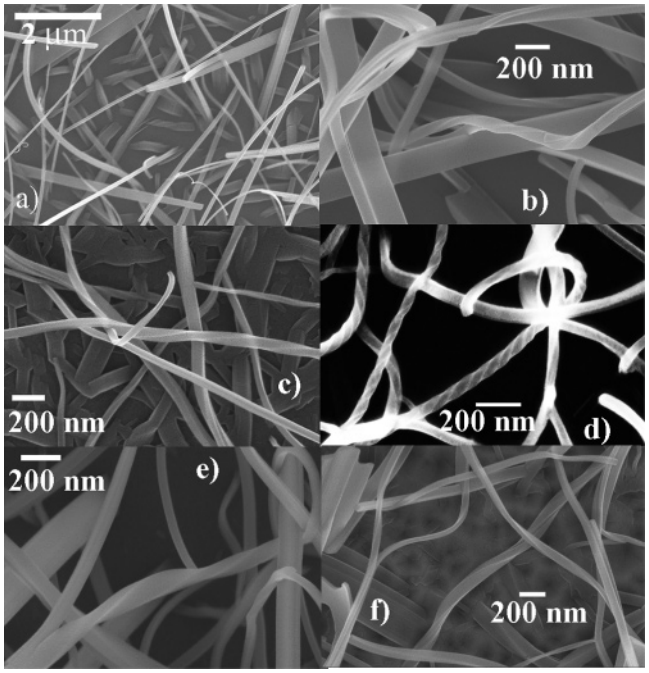

Figure 2. Representative SEM images of CuPc nanoribbons on different substrates: (a) quartz, (b) glass, (c) 10-nm CuPc film/Si (unpolished), (d) 10-nm CuPc film/indium tin oxide/glass, (e) 10-nm CuPc film/glass, and (f) 10-nm CuPc film/GaN/sapphire.

2. Experimental Section

Source materials were obtained from Fluka (CuPc, ZnPc), Strem Chemicals (FePc, NiPc, CoPc), and Aldrich (F_{16}CuPc). For CuPc, both as-received and sublimed powders were used, and no difference in obtained morphologies was observed. MPc and F_{16}CuPc nanostructures (M = Cu, Co, Fe, Ni, Zn) were fabricated by thermal evaporation of 0.04 g of source material in a three-zone tube furnace in Ar gas flow. The source temperature was 383 °C, the Ar gas flow rate was 0.3 L/min, and the pressure during growth was ∼293.3 Pa. For F_{16}CuPc, the Ar flow rate of 0.15 L/min was also attempted, and similar results were obtained as in the case of 0.3 L/min. The growth times were typically 2 and 4 h. The growth times mainly affected the total length of the nanostructures, and growth times between 10 min and 6 h were investigated. Different substrates, such as glass, Si, indium tin oxide (ITO) glass, and GaN were used. For each type of substrate, the bare substrate and the substrate covered with a thin (10-nm) CuPc film evaporated in high vacuum ($\sim 5 \times 10^{-4}$ Pa) were used. The films were evaporated using a PEVA 350T thermal evaporator.

The fabricated samples were examined by scanning electron microscopy using Leo 1530 and Zeiss Ultra 55 field-emission SEMs, by transmission electron microscopy and selected-area electron diffraction using Philips Tecnai-20 TEM and JEOL 2010F TEM instruments, by X-ray diffraction using a Bruker AXS SMART CCD diffractometer, and by absorption measurements using a Cary 50 Bio UV−vis spectrophotometer. For SEM imaging, Au (1−2 nm) was sputtered onto the samples to prevent charging effects and improve image clarity. For TEM, the samples were dispersed in an ultrasonic bath for 20 s and placed on a TEM grid (Cu with carbon film).

3. Results and Discussion

3.1. CuPc Nanoribbons and Nanowires. Figure 1 shows representative SEM images of CuPc nanostructures grown on glass substrates at different substrate temperatures. The source-to-substrate distance in this case was in the range of 26.0−33.5 cm, and the corresponding substrate temperatures were in the range 293−119 °C. Experiments at shorter source-to-substrate distances (14.5−18.5 cm, corresponding to a temperature range of 249−190 °C) yielded no significant differences in obtained morphologies at the same substrate temperature. At the highest substrate temperature (293 °C), ribbons with lengths in the range of 30−80 μm were obtained. The ribbon width and height were in the ranges ∼150−350 and ∼50−200 nm, respectively. In addition to these ribbons, large crystals with 1−3-μm widths were also observed. The substrate coverage was sparse (not shown). At a lower substrate temperature (240 °C, Figure 1a), the substrate coverage was higher, and the dimensions of the ribbons were smaller. In this case, the ribbon length was in the range of 10−15 μm, and the width was 90−190 nm for the majority of ribbons, although larger structures (length 8−13 μm, width 0.8−1.8 μm) could be found as well. Lowering the substrate temperature reduced the length of the nanostructures further, with the shortest structure (∼1 μm) being obtained at the low-temperature end. In addition to decreasing in length, the shape of the nanostructures changed, and there were more nanostructures with similar height and width (both below ∼100 nm), which could be more appropriately described as nanowires. At the lowest substrate temperature (∼119 °C, Figure 1f), elongated flat structures with occasional nanowires protruding from the surface were observed.

3.2. Twisted Nanoribbons. In addition to straight nanoribbons and nanowires, twisted nanoribbons can be observed at substrate temperatures below ∼200 °C. The appearance of twisted nanoribbons was not substrate dependent, and they were observed on a variety of substrates with and without a thin CuPc film, as shown in Figure 2. Because twisted nanoribbons that are only partly sticking out of the substrate (see Figure 1f, for example) can also be found, they are likely formed during the growth process and not as a result of electron beam exposure in the scanning electron microscope. The yield of twisted nanoribbons was the lowest on bare quartz substrate, whereas deposition of the thin (10-nm) CuPc film resulted in similar yields and morphologies on a great variety of substrates. In general, deposition of a thin CuPc film increased the yield of deposited nanostructures (both straight and twisted nanoribbons),

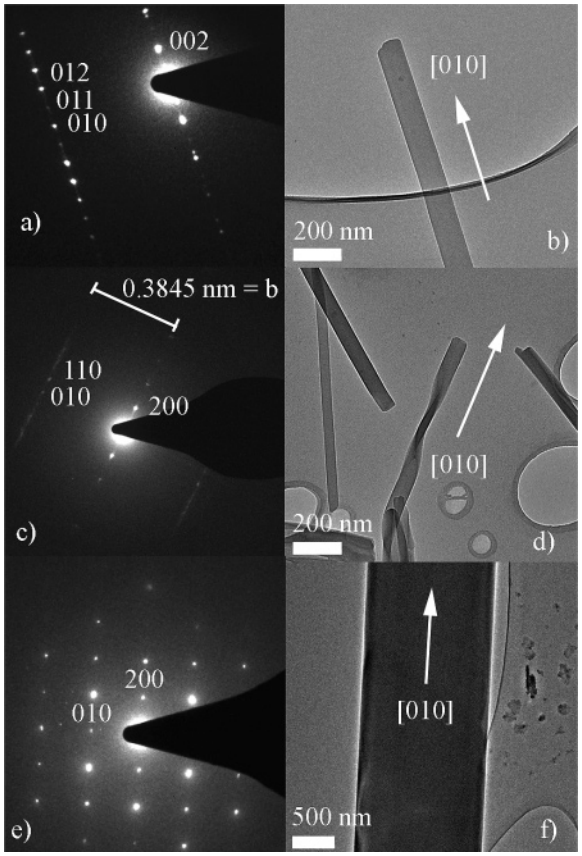

Figure 3. Representative SAED patterns and TEM images of (a,b) α-CuPc ribbon, (c,d) α-CuPc twisted ribbon, and (e,f) β-CuPc ribbon. The labeled growth direction was determined by measuring lattice spacings from SAED patterns. The tilt between the TEM image and the corresponding SAED pattern is due to the imaging system of the TEM used.

but had no significant effect on the types of morphologies observed. Both left-handed and right-handed twisted nanoribbons were found. To obtain more information about the growth of these structures, transmission electron microscopy (TEM) measurements were performed. Representative selected-area electron diffraction (SAED) patterns and corresponding TEM images are shown in Figure 3. Depending on the substrate temperature, α- or β-phase CuPc could be obtained. Phthalocyanine materials can have several polymorphs, such as α, β, γ, and *x* phases.[27,37] The most commonly studied forms are the α and β polymorphs. In both polymorphs, planar phthalocyanine molecules are stacked along the stacking *b* axis. The main difference between the two polymorphs is the tilt angle of the phthalocyanine molecular plane with respect to the stacking axis,[27,30] which is 26.5° in the α phase and 46.8° in the β phase.[30] The molecules in neighboring stacks are roughly orthogonal, forming a herringbone arrangement. It can be observed from Figure 3f that the long ribbons of β-phase CuPc grow along the *b* axis, which is the stacking axis of the phthalocyanine molecules, similar to previously reported results.[12] The α-phase CuPc nanostructures also typically grow along the [010] direction as shown in Figure 3b and d, but they have a considerably smaller size than the β-phase ribbons. The twisted nanoribbons occur only for the α-phase CuPc, and the twisting structure remains intact after detachment from the substrate and subsequent dispersion and placement on the TEM grid. The twisted ribbon morphology is not limited to CuPc, and it has been observed for other metal phthalocyanines, as shown in Figure 4. For CoPc, NiPc, FePc, and ZnPc, twisted ribbons occurred

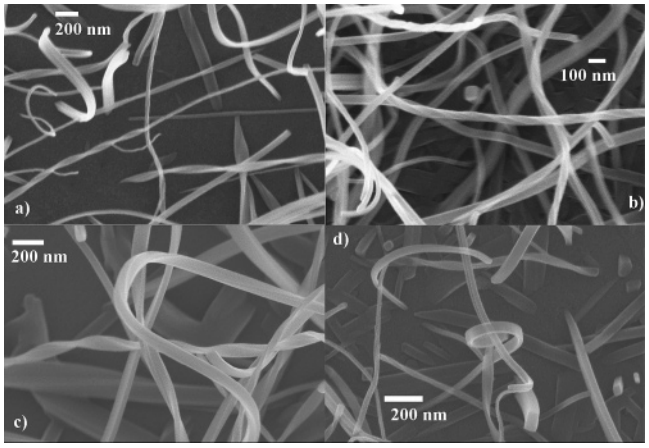

Figure 4. Representative SEM images of twisted ribbons of (a) FePc, (b) CoPc, (c) NiPc, and (d) ZnPc.

only at lower substrate temperatures, similarly to CuPc. The yield of twisted ribbons for all metal phthalocyanines (MPcs) was in the range 15−30%. In general, the dependences of the morphology on the substrate temperature are similar for all phthalocyanine materials studied. The nanostructures follow the same trend of increased size with increasing temperature, and there is a phase transition from α to β phase with increasing temperature. In general, ribbons with lengths in the range of several tens of micrometers were observed at high substrate temperatures (191−240 °C), whereas at low substrate temperatures (71−119 °C), thin nanoribbons/nanowires with lengths in the range of 0.5−2 μm and widths of <100 nm were found. However, the exact substrate temperature at which certain morphologies/crystal structures were observed showed small variation for different materials, because the temperatures for the α-to-β phase transition were not identical for all of the materials investigated.

The mechanism of formation of twisted nanoribbons is difficult to elucidate, as it is difficult to obtain clear SAED patterns because of the twisting structure of the ribbon. Helical nanostructures were previously reported for a number of different materials.[43−58] It is known that phthalocyanine derivatives containing chiral carbons in the side chain can form a mesophase twisting arrangement of the CuPc planes,[43,58] but no twisting MPc (M = Cu, Co, Fe, Ni, Zn) structures were previously reported. Also, the common mechanism of formation of helical[46,47,52] and twisted[47] nanostructures where coiling is induced by the catalyst is not applicable in this case because no catalyst was used and CuPc nanostructures grow by a vapor−solid mechanism[12] and not a vapor−liquid−solid mechanism. Formation of helices and spirals due to polar surfaces[45,48] is also not applicable to the formation of metal phthalocyanine twisted nanoribbons. Another reported mechanism for the formation of a helical structure is the twisting of superlattice-structured ZnO nanobelts, where twisting was induced by a small rotation between the growth direction of the two stripes in the superlattice.[44] The superlattice consisted of periodic nanostripes (period = 3.5 nm) that were oriented almost parallel (∼5° offset) to the growth direction and whose *c* axes were roughly perpendicular to each other.[44] It should be noted that MPc nanoribbons grown along the stacking axis (*b* axis) have a herringbone arrangement with molecular planes in neighboring stacks roughly perpendicular to each other. Thus, mechanisms similar to twisting induced by a superlattice structure might also play a role in the formation of twisted MPc nanoribbons. However, in this case, twisted nanoribbons instead of helices were formed. The obtained morphology is similar to twisted organic nano-

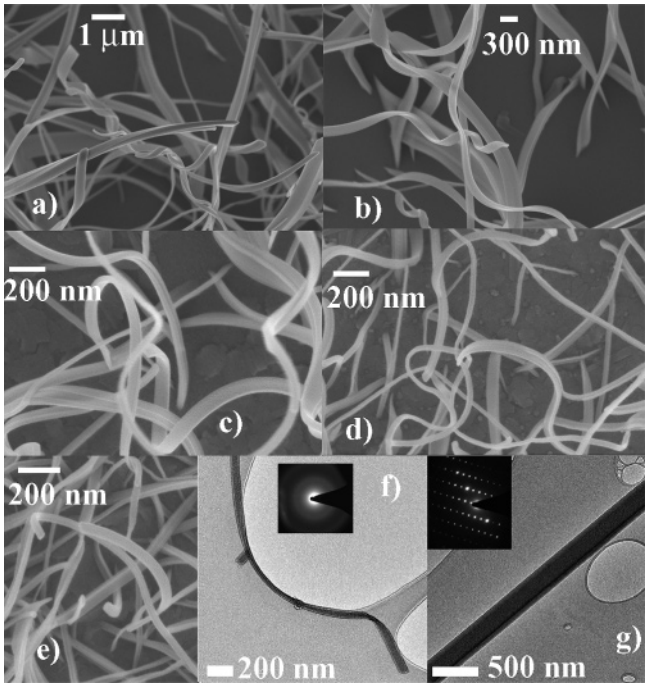

Figure 5. Representative SEM images of F_{16}CuPc nanostructures on indium tin oxide/glass substrates grown at substrate temperatures of (a) 293, (b) 273, (c) 240, (d) 216, and (e) 195 °C and TEM images of F_{16}CuPc nanoribbons grown at (f) 195 and (g) 273 °C, with the insets in f and g showing representative SAED patterns.

ribbons obtained in solutions after gelation.[49−51,54−57] It has been shown that dendron rod-coil molecules assemble into flat or twisted ribbons depending on the solvent.[49,50] The twisted ribbons could also be formed by gelation of 2-acryloylamide-dodecane-1-sulfonic acid[51] or oligo(*p*-phenylene vinylene) (OPV).[54−56] In the latter case, comparatively larger nanoribbons were obtained, with thicknesses of 12−20 nm and widths of 50−200 nm.[54] The ribbons were formed by lamellar packing of OPV units through hydrogen-bonding, $\pi-\pi$-stacking, and van der Waals interactions.[54] Although the fabrication process of our MPc nanoribbons is entirely different, the crystal packing of MPcs also consists of stacks of planar molecules. The angle between molecular planes in neighboring stacks of molecules is greater than 90° (whereas for the β phase, it is close to 90°), and the distance between stacks with the same molecule orientation is $a = 2.39$ nm.[30] This value is similar to the period of the superlattice in ZnO helices,[44] although in the case of CuPc nanoribbons, the helix diameter is zero, i.e., twisted nanoribbons are obtained. The reason no twisted ribbons are obtained in the case of the β phase is that β-phase ribbons have larger dimensions and, consequently, a flat geometry is more stable than a helical geometry for the β phase.

3.3. Copper Hexadecafluorophthalocyanine Nanowires and Nanoribbons. The dependence of the morphology of F_{16}-CuPc nanostructures on the substrate temperature is shown in Figure 5. Representative TEM images with corresponding SAED patterns of nanoribbons from the low- and high-temperature ends are also shown. In this case as well, we can observe a similar trend of reduced size with reducing substrate temperature. However, several significant differences can be observed compared to the MPc nanoribbons and nanowires. First, formation of nanohelices was observed upon exposure to an electron beam even at low voltages of 1−3 kV. This issue is discussed in more detail in the following section. Second, no twisted nanoribbons were found. Third, whereas nanoribbons grown at high substrate temperatures exhibit excellent crystallinity, this is not the case

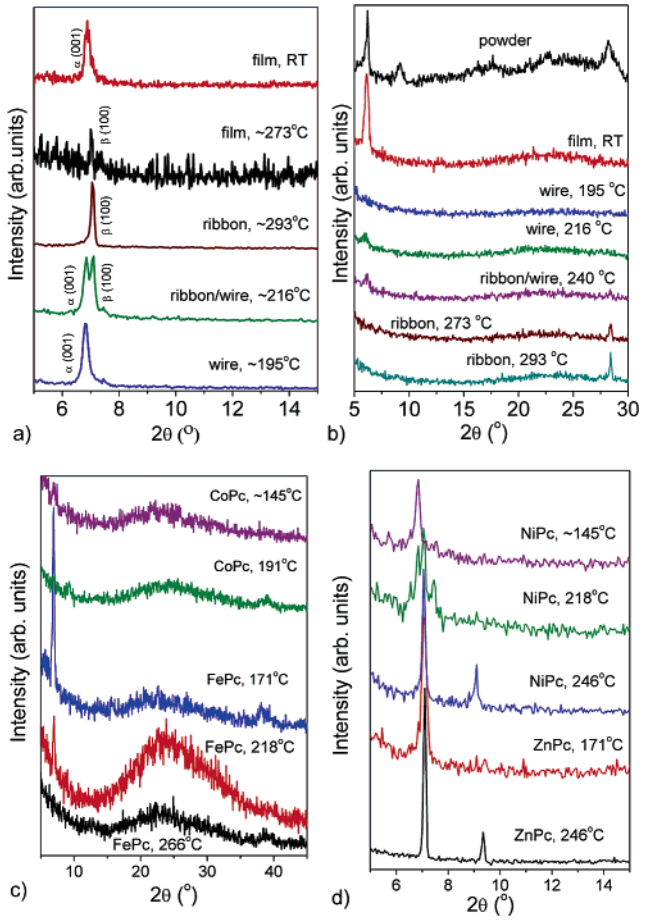

Figure 6. Representative XRD patterns of different phthalocyanines at different substrate temperatures: (a) CuPc, (b) F_{16}CuPc, (c) FePc and CoPc, (d) ZnPc and NiPc.

for those grown at low substrate temperatures. The ribbons grown at higher substrate temperatures are single-crystalline, and based on the similarity of crystal structure with that of CuPc, the growth direction is likely also [010].

3.4. XRD and Absorption Measurements. To study the crystal phases of the fabricated materials in more detail, XRD and absorption measurements were performed, with the results shown in Figures 6 and 7, respectively. Obvious differences can be observed in the XRD spectra for different substrate temperatures. This is not surprising, because it is well-known that the crystalline structure of metal phthalocyanines is dependent on the deposition or annealing temperature[25,27,28] and the phase transformation can also be induced by exposure to solvent vapor.[26,29] Phthalocyanine thin films can also show some preferential ordering, which is affected by the film thickness.[27] The deposition conditions (e.g., temperature, deposition rate) are also known to affect the ordering in phthalocyanine thin films,[17,30,32] which likely accounts for the appearance of different XRD peaks at different substrate temperatures. Although MPcs are known to form similar crystals,[35,36] there are differences between the obtained crystal structure and the optical properties at the same substrate temperature for different MPcs. For example, thin films deposited at room temperature for CuPc are in the α phase,[27,37] whereas those of ZnPc are amorphous.[34] On the other hand, polycrystalline ZnPc films are obtained when the substrate temperature is 373 K.[34] A transformation to β-ZnPc was observed after annealing at ~240 °C.[30] For CuPc, annealing at a temperature of 290 °C resulted in a complete transformation from the α phase to the β phase, whereas deposition at substrate temperatures above 210 °C resulted in β-phase films.[25] The

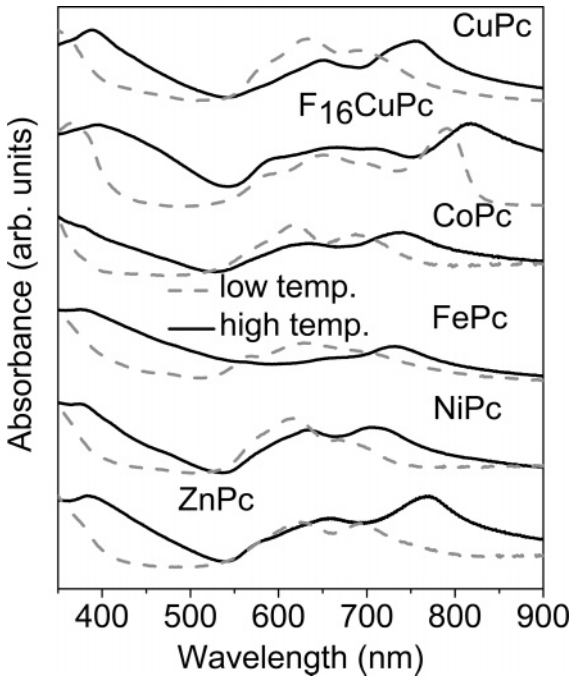

Figure 7. Absorption characteristics of different metal phthalocyanine thin films. Representative spectra for samples deposited at low and high substrate temperatures are given for each material. The substrate temperatures were as follows: CuPc, 216 and 170 °C; F_{16}CuPc, 273 and 195 °C; CoPc, 191 and 120 °C; FePc, 218 and 120 °C; NiPc, 191 and 120 °C; and ZnPc, 191 and 120 °C.

α-to-β transformation in FePc was reported at substrate temperatures of ∼250 °C.[28] Thus, some differences are expected between different MPcs at the same substrate temperature. The clearest transition from the α to β phase was observed for CuPc and NiPc. The XRD spectra obtained for CuPc (Figure 6a) are in good agreement with previous reports.[27,37] The highest and lowest substrate temperatures for NiPc and CuPc yielded pure β and α phases, respectively, whereas mixtures were observed at intermediate temperatures. In ZnPc, CoPc, and FePc, the XRD spectra showed more gradual transitions and, in some cases, the appearance of new peaks corresponding to the same crystal phase, which is likely due to the dependence of preferential ordering on substrate temperature. However, from the red shift of the Q-band in the absorption spectra, the phase transformation is obvious for all materials studied. The absorption spectra obtained for the nanostructures deposited at low and high substrate temperatures are in good agreement with previously reported absorption spectra for α- and β-phase CuPc, NiPc, CoPc, and ZnPc,[19] as well as α-phase FePc.[21,23]

F_{16}CuPc shows very different behavior. No significant peaks were observed for the nanostructures deposited at the low-temperature end (Figure 6b), in agreement with the SAED patterns indicating poor crystallinity of F_{16}CuPc nanowires/nanoribbons deposited at low substrate temperatures. Because twisted nanoribbons of MPcs occur only at low substrate temperatures where α-phase nanoribbons/wires are grown, the absence of single-crystalline nanoribbons/wires in this temperature region in the case of F_{16}CuPc is probably the reason for the absence of twisted nanoribbons. The dominant X-ray diffraction peak for the F_{16}CuPc film at ∼6.1° is in good agreement with previously reported values.[39] A similar peak at much lower intensity can be obtained for wires grown at higher substrate temperatures (216 and 240 °C), whereas a further increase of substrate temperature results in the disappearance of this peak and the appearance of a new peak that possibly corresponds to β (311). The prominent absorption maxima of F_{16}CuPc nanostructures and films are located at 650 and 790 nm, which is in good agreement with previously reported values of 654 and 796 nm.[38] The nanostructure absorption spectrum are somewhat broader than that of the film, which is likely due to their inferior crystallinity as confirmed by XRD and SAED. Furthermore, F_{16}CuPc ribbons deposited at high substrate temperature exhibit a red shift of the absorption maximum to 818 nm, indicating a possible phase transformation similar to that observed in MPcs. The appearance of a prominent absorption peak at ∼820 nm has previously been observed in F_{16}ZnPc after annealing at 453 K, which also resulted in improved crystallinity of the samples.[59]

3.5. Effects of Electron Beam Exposure. It has been shown that β-CuPc nanoribbons exhibit excellent flexibility when manipulated with mechanical probes.[12] Figure 8 illustrates the flexibility of CuPc nanoribbons in as-grown samples, with high-curvature ribbons clearly observed. Under exposure to an electron beam, curving of the nanoribbons can be observed even at a relatively low voltage of 3 kV. The coiling of nanoribbons is typically observed only in thin nanoribbons. It has been

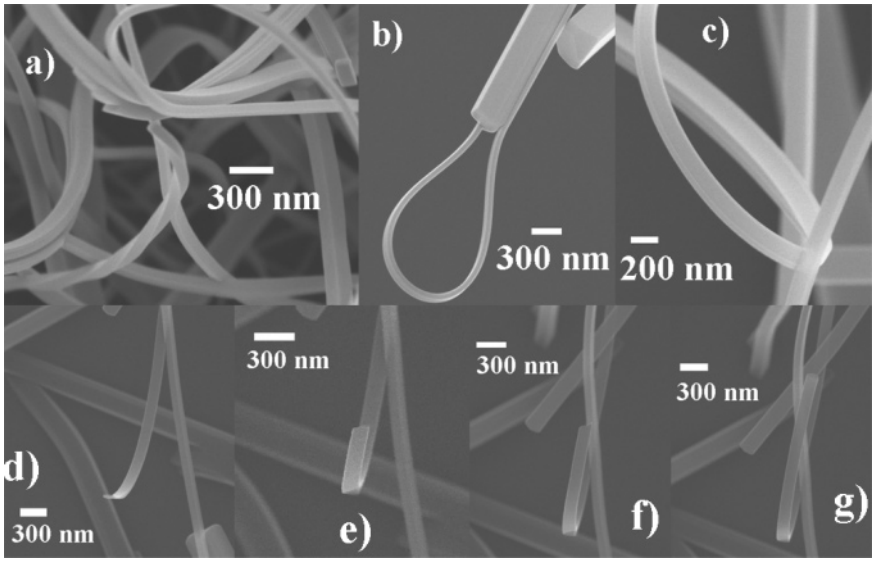

Figure 8. Representative SEM images illustrating the high flexibility of CuPc nanoribbons: (a−c) high-curvature ribbons found in the sample, (d−g) curving of the CuPc nanoribbons upon electron beam exposure.

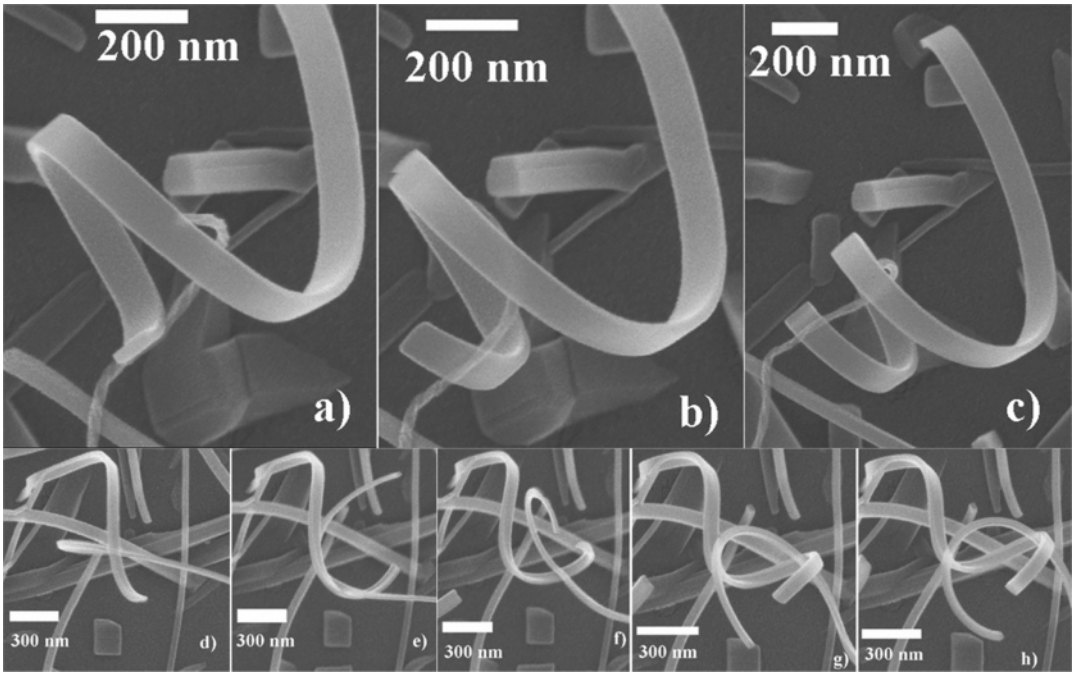

Figure 9. Representative SEM images illustrating the curving of ZnPc nanoribbons, with panels a−c and d−h depicting two different sequences.

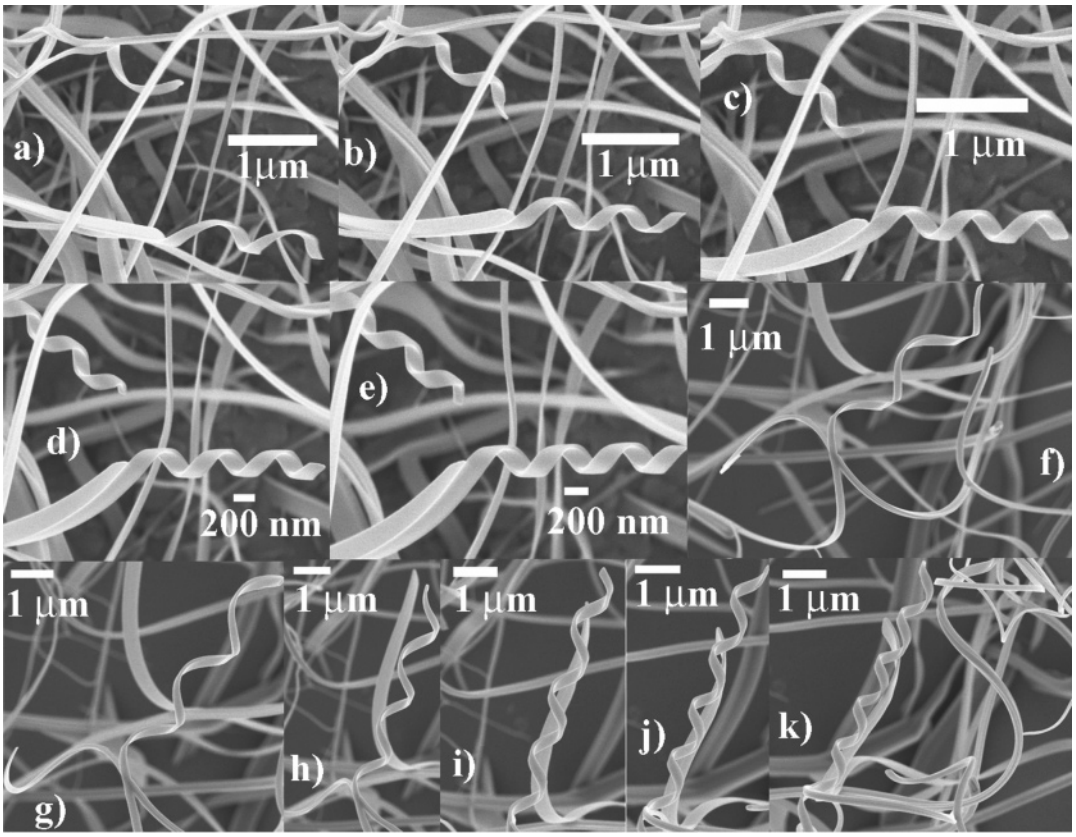

Figure 10. Representative SEM images illustrating the formation of $F_{16}CuPc$ helices upon electron beam exposure, with panels a−e and f−k depicting two different coiling sequences.

previously shown that nanoribbons with smaller dimensions (width and height below ∼150 nm) retained their folded shape when force was removed, unlike large ribbons, which were able to recover their original morphology.[12] Similar behavior was observed in other MPcs, with the most pronounced coiling effect observed for ZnPc, as illustrated in Figure 9. In all cases, the most pronounced coiling effects were observed in thin nanoribbons with heights of less than ∼40 nm. However, $F_{16}CuPc$ exhibits different behavior upon exposure to an electron beam, as shown in Figure 10. In this case, we can observe considerably more pronounced coiling, with the formation of regular helices. The helix radius and pitch depend on the starting geometry of the nanoribbon and the time of exposure to the electron beam. The coiling process is self-limiting, i.e., once a certain helix geometry is reached, there is no further coiling of the ribbon. Recent theoretical modeling of elastic properties of thin anisotropic nanoribbons has shown that both nanohelices and twisted nanoribbons can be energetically favorable compared to a flat

geometry under certain conditions.[60] Whereas detailed theoretical descriptions of the formation of ZnO nanohelices as a result of competition between elastic energy, surface-polarization-induced energy, volume energy, and defect-induced energy are available,[61] no such calculations exist for organic molecule nanoribbons. On the basis of the experimental data, it was proposed that the ZnO nanohelices were formed as a result of minimization of the total energy consisting of elastic and spontaneous polarization contributions.[48] The total energy was found to depend on the nanostructure dimensions, and the critical thickness of the ZnO belts was found to be ~15 nm. For thicknesses less than this value, a coiled structure was more energetically favorable, whereas for thicker belts, a straight geometry was the stable shape.[48] A similar phenomenon was observed for the coiling of phthalocyanine nanoribbons: coiling was only observed in very thin nanoribbons. Compared to MPcs, thin nanoribbons are more commonly found in F_{16}CuPc samples. In addition, F_{16}CuPc is an electron-acceptor molecule, because of the electron-withdrawing fluorine atoms. Thus, there is a possibility that exposure of the F_{16}CuPc to an electron beam would result in changes in the electrostatic energy and consequent rolling of the nanoribbons to form helices in order to minimize the total energy. It should be noted that another possible explanation for nanohelix formation could be heating of the samples. F_{16}CuPc nanostructures decompose when exposed to an electron beam under a voltage of 20 kV. Because the decomposition temperature of F_{16}CuPc is 550 °C,[62] it is unlikely that there are considerable heating effects at voltages of 1−3 kV. Therefore, the formation of helices due to heating of the sample is not a likely formation mechanism. Further studies, including detailed characterization of the elastic properties of MPcs and F_{16}CuPc, are needed to conclusively establish the mechanism of nanohelix formation upon exposure to an electron beam. Excellent flexibility and easy formation of helices inside a scanning electron microscope indicates that phthalocyanine nanostructures might represent a low-cost and low-temperature alternative to inorganic nanostructures for applications in functional components of NEMS and MEMS (nano- and microelectromechanical systems, respectively), sensors, and transducers.

4. Conclusion

Nanoribbons and nanowires of different p-type phthalocyanines (CuPc, NiPc, CoPc, FePc, and ZnPc) and an n-type phthalocyanine derivative (F_{16}CuPc) were fabricated by the organic vapor-phase deposition method. In all investigated materials, substrate temperature strongly affected the morphology and crystal structure of the fabricated nanostructures. For MPcs (M = Co, Cu, Fe, Ni, Zn), straight and twisted α-phase nanoribbons and nanowires were obtained for lower substrate temperatures, whereas for β-phase structures, only straight nanoribbons are found. However, no twisted F_{16}CuPc nanoribbons were obtained, which was attributed to poor crystallinity of F_{16}CuPc nanoribbons and nanowires deposited at low substrate temperatures. However, upon exposure to an electron beam, F_{16}CuPc nanohelices formed. Because of the variety of morphologies and different properties of different crystal structures, fabricated phthalocyanine materials are of interest for a variety of applications from organic electronic and optoelectronic devices to sensors and transducers.

Acknowledgment. The work reported in this article was supported by the Research Grants Council of The Hong Kong Special Administrative Region, China (Project 7010/05P). Financial support from the Strategic Research Theme, University Development Fund, and Seed Funding Grant (administrated by The University of Hong Kong) are also acknowledged. The authors thank Y. F. Chan from Electron Microscopy Unit, University of Hong Kong, for his help in obtaining TEM images.

References and Notes

(1) Wöhrle, D.; Kreienhoop, L.; Schlettwein, D. Phthalocyanines and related Macrocycles in Organic Phototovoltaic Junctions. In *Phthalocyanines, Properties, and Applications*; Leznoff, C. C., Lever, A. B. P., Eds.; VCH Publishers Inc.: New York, 1996; pp 219−284.
(2) Peumans, P.; Bulović, V.; Forrest, S. R. *Appl. Phys. Lett.* **2000**, *76*, 2650.
(3) Yang, F.; Shtein, M.; Forrest, S. R. *Nature Mater.* **2005**, *4*, 37.
(4) Blochwitz, J.; Pfeiffer, M.; Fritz, T.; Leo, K. *Appl. Phys. Lett.* **1998**, *73*, 729.
(5) Zhou, X.; Pfeiffer, M.; Blochwitz, J.; Werner, A.; Nollau, A.; Fritz, T.; Leo, K. *Appl. Phys. Lett.* **2001**, *78*, 410.
(6) Kao, P. C.; Chu, S. Y.; You, Z. X.; Liou, S. J.; Chuang, C.-A. *Thin Solid Films* **2006**, *498*, 249.
(7) Fujii, N.; Ohmori, Y.; Yoshino, K. *IEEE Trans. Electron Devices* **1997**, *44*, 1204.
(8) Ben Chabane, R.; Ltaief, A.; Dridi, C.; Rahmoouni, H.; Bouazizi, A.; Ben Ouada, H. *Thin Solid Films* **2003**, *427*, 371.
(9) Zhang, J.; Wang, H.; Yan, X.; Wang, J.; Shi, J.; Yan, D. *Adv. Mater.* **2006**, *17*, 1191.
(10) Wang, J.; Wang, H.; Yan, X.; Huang, H.; Yan, D. *Appl. Phys. Lett.* **2005**, *87*, 093507.
(11) de Boer, R. W. I.; Stassen, A. F.; Craciun, M. F.; Mulder, C. L.; Molinari, A.; Rogge, S.; Morpugo, A. F. *Appl. Phys. Lett.* **2005**, *86*, 262109.
(12) Tang, Q.; Li, H.; He, M.; Hu, W.; Liu, C.; Chen, K.; Wang, C.; Liu, Y.; Zhu, D. *Adv. Mater.* **2006**, *18*, 65.
(13) Bouvet, M. *Anal. Bioanal. Chem.* **2006**, *384*, 366.
(14) Nagasawa, T.; Murakami, K.; Watanabe, K. *Mol. Cryst. Liq. Cryst.* **1998**, *316*, 389.
(15) Newton, M. I.; Starke, T. K. H.; Willis, M. R.; McHale, G. *Sens. Actuators B* **2000**, *67*, 307.
(16) Schechtman, B. H.; Spicer, W. E. *J. Mol. Spectrosc.* **1970**, *33*, 28.
(17) Debe, M. K. *J. Vac. Sci. Technol. A* **1992**, *10*, 2816.
(18) Ritz, A.; Lüth, H. *Appl. Phys. A* **1983**, *31*, 75.
(19) Lucia, E. A.; Verdearme, F. D. *J. Chem. Phys.* **1968**, *48*, 2674.
(20) Laurs, H.; Heiland, G. *Thin Solid Films* **1987**, *149*, 129.
(21) Davidson, A. T. *J. Chem. Phys.* **1982**, *77*, 168.
(22) Edwards, L.; Gouterman, M. *J. Mol. Spectr.* **1970**, *33*, 292.
(23) Djurišić, A. B.; Kwong, C. Y.; Lau, T. W.; Liu, Z. T.; Kwok, H. S.; Lam, L. S. M.; Chan, W. K. *Appl. Opt.* **2003**, *42*, 6382.
(24) Resel, B.; Ottmar, M.; Hanack, M.; Keckes, J.; Leising, B. *J. Mater. Res.* **2000**, *15*, 934.
(25) Maggioni, G.; Quaranta, A.; Carturan, S.; Patelli, A.; Tonezzer, M.; Ceccato, R.; Della Mea, G. *Chem. Mater.* **2005**, *17*, 1895.
(26) Brinkmann, M.; Wittmann, J. C.; Chaumont, C.; Andre, J. J. *Thin Solid Films* **1997**, *292*, 192.
(27) Berger, O.; Fischer, W. J.; Adolphi, B.; Tierbach, S.; Melev, V.; Schreiber, J. *J. Mater. Sci.: Mater. Electron.* **2000**, *11*, 331.
(28) Miller, C. W.; Sharoni, A.; Liu, G.; Colesniuc, C. N.; Fruhberger, B.; Schuller, I. K. *Phys. Rev. B* **2005**, *72*, 104113.
(29) Iwatsu, F. *J. Phys. Chem.* **1988**, *92*, 1678.
(30) Gould, R. D. *Coord. Chem. Rev.* **1996**, *156*, 237.
(31) Bayliss, S. M.; Heutz, S.; Cloots, R.; Middleton, R. L.; Rumbles, G.; Jones, T. S. *Adv. Mater.* **2000**, *12*, 202.
(32) Debe, M. K.; Pourier, R. J.; Kam, K. K. *Thin Solid Films* **1991**, *197*, 335.
(33) Komiyama, M.; Sakakibara, Y.; Hirai, H. *Thin Solid Films* **1987**, *151*, L109.
(34) Senthilarasu, S.; Velumani, S.; Sathyamoorthy, B.; Subbarayan, A.; Ascencio, J. A.; Canizal, G.; Sebastián, P. J.; Chavez, J. A.; Perez, B. *Appl. Phys. A* **2003**, *77*, 383.
(35) Monteath Robertson, J. *J. Chem. Soc.* **1935**, *1935*, 615.
(36) Ashida, M.; Uyeda, N.; Suito, E. *Bull. Chem. Soc. Jpn.* **1966**, *39*, 2616.
(37) Prabakaran, R.; Kesavamoorthy, R.; Reddy, G. L. N.; Xavier, F. P. *Phys. Status Solidi B* **2002**, *229*, 1175.
(38) Basova, T.; Kol'tsov, E.; Hassan, A.; Tsargorodskaya, A.; Ray, A.; Igumenov, I. *Phys. Status Solidi B* **2005**, *242*, 822.
(39) Bao, Z.; Lovinger, A. J.; Brown, J. *J. Am. Chem. Soc.* **1998**, *120*, 207.
(40) Xu, H. B.; Chen, H. Z.; Xu, W. J.; Wang, M. *Chem. Phys. Lett.* **2005**, *412*, 294.
(41) Laudise, R. A.; Kloc, Ch.; Simpkins, P. G.; Siegrist, T. *J. Cryst. Growth* **1998**, *187*, 449.

(42) Stein, M.; Gossenberger, H. F.; Benziger, J. B.; Forrest, S. R. *J. Appl. Phys.* **2001**, *89*, 1470.
(43) Kobayashi, N. *Coord. Chem. Rev.* **2001**, *219*−*221*, 99.
(44) Gao, P. X.; Ding, Y.; Mai, W.; Hughes, W. L.; Lao, C.; Wang, Z. L. *Science* **2005**, *309*, 1700.
(45) Yang, R.; Wang, Z. L. *J. Am. Chem. Soc.* **2006**, *128*, 1466.
(46) Bae, S. Y.; Lee, J.; Jung, H.; Park, J.; Ahn, J.-P. *J. Am. Chem. Soc.* **2005**, *127*, 10802.
(47) Yang, S.; Chen, X.; Motojima, S. *Diamond Relat. Mater.* **2004**, *13*, 2152.
(48) Kong, X. Y.; Wang, Z. L. *Nano Lett.* **2003**, *3*, 1625.
(49) Sone, E. D.; Zubarev, E. R.; Stupp, S. I. *Small* **2005**, *1*, 694.
(50) Sone, E. D.; Zubarev, E. R.; Stupp, S. I. *Angew. Chem., Int. Ed.* **2002**, *41*, 1706.
(51) Zhan, C.; Wang, J.; Yuan, J.; Gong, H.; Liu, Y.; Liu, M. *Langmuir* **2003**, *19*, 9440.
(52) McIlroy, D. N.; Alkhateeb, A.; Zhang, D.; Aston, D. E.; Marcy, A. C.; Norton, M. G. *J. Phys: Condens. Matter* **2004**, *16*, R415.
(53) Ajayaghosh, A.; Vijayakumar, C.; Varghese, R.; George, S. J. *Angew. Chem., Int. Ed.* **2006**, *45*, 456.
(54) George, S. J.; Ajayaghosh, A. *Chem. Eur. J.* **2005**, *11*, 3217.
(55) Ajayaghosh, A.; George, S. J.; Praveen, V. K. *Angew. Chem., Int. Ed.* **2003**, *42*, 332.
(56) Ajayaghosh, A.; Varghese, R.; George, S. J.; Vijayakumar, C. *Angew. Chem., Int. Ed.* **2006**, *45*, 1141.
(57) Ajayaghosh, A.; George, S. J. *J. Am. Chem. Soc.* **2001**, *123*, 5148.
(58) Engelkamp, H.; Middelbeek, S.; Nolte, R. J. M. *Science* **1999**, *284*, 785.
(59) Schlettwein, D.; Graaf, H.; Meyer, J.-P.; Oekermann, T.; Jaeger, N. I. *J. Phys. Chem. B* **1999**, *103*, 3078.
(60) Iglič, A.; Tzaphlidou, M.; Remškar, M.; Babnik, B.; Daniel, M.; Kralj-Iglič, V. *Fullerenes, Nanotubes, Carbon Nanostruct.* **2005**, *13*, 183.
(61) Tu, Z. C.; Li, Q. X.; Hu, X. *Phys. Rev. B* **2006**, *73*, 115402.
(62) Kol'tsov, E.; Basova, T.; Semyannikov, P.; Igumenov, I. *Mater. Chem. Phys.* **2004**, *86*, 222.